Monthly Notices of the ROYAL ASTRONOMICAL SOCIETY

MNRAS **537,** 3100–3108 (2025) https://doi.org/10.1093/mnras/staf225
Advance Access publication 2025 February 07

Characterization of H_2O:N_2 ice under bombardment by cosmic rays – I. Reaction rates and chemical equilibrium

L. M. S. V. Queiroz,[1]★ J. R. C. Silva,[1] L. F. A. Ferrão[1] and S. Pilling[2]

[1]*Departamento de Química, Instituto Tecnológico de Aeronáutica (ITA), São José dos Campos, SP, 12228-900, Brazil*
[2]*Laboratório de Astroquímica e Astrobiologia (LASA), Instituto de Pesquisa e Desenvolvimento (IPD), Universidade do Vale do Paraíba (UNIVAP), São José dos Campos, SP, 12244-000, Brazil*

Accepted 2025 February 3. Received 2025 January 29; in original form 2024 November 27

ABSTRACT

In space, nitrogen-rich ice is constantly exposed to ionizing radiation, which triggers chemical reactions and desorption processes allowing a chemical enhancement of interstellar medium (ISM). Here, we present the first part of a series of studies on the effect of cosmic ray bombardment (40 MeV Ni^{11+} ions) on H_2O:N_2 (1:5) ice at 15 K, employing the PROCODA code as the modelling tool including 28 chemical species and 930 chemical coupled equations (also including desorption). This first part focuses on the reaction rates and chemical equilibrium stage due to radiation processing. Among the results, we characterize the molecular abundances at chemical equilibrium, including experimentally observed and non-observed species (predicted) suggesting some candidates as a target for astronomical observation. The best-fitting models provided the effective rate coefficients, which can be employed in astrochemical models to understand the chemistry of cold space environments. The findings also help to clarify the chemical processes of N-bearing species in the ISM and frozen surfaces of the Solar system, including the moon of giant planets, outer solar system objects, and ices in the interstellar and protostellar medium.

Key words: astrochemistry – molecular data – molecular processes – methods: data analysis – software: data analysis – ISM: molecules.

1 INTRODUCTION

Diatomic nitrogen is believed to be the most abundant nitrogen-bearing species in the interstellar medium (ISM) and at the surfaces of Transneptunian objects, such as Triton and Pluto (Cruikshank et al. 1993; Quirico et al. 1999; Vasconcelos et al. 2017b). However, as N≡N is a homonuclear molecule that presents a strong triple bond, it is 'near-transparent' to infrared analysis and other 'low-energy' radiation sources commonly available in the space. In this sense, its identification is generally carried out in an indirect way by the identification of its 'daughter' species, such as N_2H^+, NH_3, and OCN^-, which are generated by the interactions within the nitrogen-containing ices and/or with radiation sources. Furthermore, the identification of nitrogen-bearing species may give insights on the formation of important structures, as simple amino acids (Vasconcelos et al. 2017a).

Water ices containing N_2 have been studied in an attempt to clarify the presence of N-bearing molecules in space (de Barros et al. 2015; Hudson 2018). Such ices in the presence of ionizing radiation have their chemical complexity enhanced due to the input of energy that allows chemical reactions to produce new species and desorption processes.

Among the experimental studies of H_2O:N_2 ices is the work of de Barros with the extension from the work of Hudson (2018), which simulates the effects of cosmic rays in these ices with several implications on astrochemistry.

In the current research, we employ the PROCODA (Pilling, Carvalho & Rocha 2022; Pilling et al. 2023a) code to understand the chemical evolution of H_2O:N_2 (1:5) ice irradiated by 40 MeV Ni^{11+} at 15 K, using the experimental data from from Barros et al. (2015), taking into account the considerations pointed out by Hudson. The PROCODA code solves a system of chemically coupled differential equations applied for astrochemistry research. It can provide the effective rate constants (ERCs) for direct radiation-induced and bimolecular reactions, as well as the chemical equilibrium (CE) phase within the ice that emerges at higher radiation levels. It also offers insights into the abundances of observed and unobserved (or unknown) species in infrared (IR) spectra during the ice's chemical evolution under radiation.

Here, we considered in the ice 28 possible species (H, H_2, N, O, OH, NH_3, H_2O, NH_4, H_3O, N_2, N_2H_2, NO, HNO, O_2, HO_2, H_2O_2, N_3, N_2O, NO_2, HNO_2, O_3, HO_3, N_2O_2, NO_3, HNO_3, N_2O_3, N_2O_4, and N_2O_5) and a total of 930 coupled chemical (including also desorption equations). From all the 28 species, only five were observed in the experiment by IR spectroscopy: N_2, H_2O, NO, NO_2, and N_2O, the other 22 were named non-observed or predicted species.

This work is the first part of a series of studies on the effect of cosmic ray bombardment on H_2O:N_2 (1:5) ice, employing the PROCODA code as the modelling tool. This first part is focused on the reaction rates and chemical equilibrium stage due to radiation

★ E-mail: vetrano.leticia@gmail.com

processing. Part 2 will focus on kinetics and the influence of radiation dose and chemical environments on chemical reactions as well as reaction mechanisms, and Part 3 will focus on chemical desorption processes and implications for N-bearing molecular detections in gas phase.

2 METHODOLOGY

In this section, we provide details on the employed experimental data (and its handling) and the details of the PROCODA code itself.

2.1 The experimental data

The employed experimental data was obtained from Barros et al. (2015), by Fourier transform infrared (FTIR) absorption spectroscopy analysis of a N_2:H_2O ice, with a ratio of 5:1 (although the authors reported an initial ratio of 10:1 for N_2:H_2O, their column density values show a ratio of 5:1), processed by 40 MeV Ni^{11+} at 15 K at Ganil Laboratory, France. Pure water and nitrogen gases were mixed and deposited over the a CsI substrate, inside a high vacuum chamber. The ice thickness was calculated by the authors and considered to be 0.62 μm.

From their results N_3, NO, NO_2, NO_3, N_2O, N_2O_2, N_2O_3, N_2O_4, N_2O_5, O_3, HNO, HNO_2, and HNO_3 are the observed species, although HNO, HNO_2, and HNO_3 were not quantified. However, Hudson (2018) made a critical overview of de Barros's work, in which it was pointed out that some IR bands could be misattributed or even that some species should not exist, and the observed data related to them are a consequence of a CO_2 contamination at Barros et al. (2015) experiment. In his work, Hudson considered that three out of the 10 quantified species (NO, NO_2, and N_2O) were reliable.

It is important to note that while Barros et al. (2015) made use of a fast nickel ion beam to irradiate the ice, Hudson (2018) used H^+. As expected, different beams should lead to different results. In light of the diverse astronomical environments in which ices are discovered, it is crucial to investigate potential combinations of temperature, radiation doses, and radiation type. Nevertheless, the simulation of all these possibilities in terrestrial laboratories to obtain details about the chemical evolution within the ice may prove to be impractical.

In this work, only the three species considered by Hudson (2018) were utilized as experimental input data for the PROCODA. The provided data set comprises 9 to 11 pairs of points, each consisting of the column density of a specific observed species and the corresponding irradiation time. Specifically, the data set includes 11 pairs for N_2 and H_2O species, 10 pairs for N_2O and NO_2 species, and 9 pairs for NO species. To enhance the accuracy of the model, for each observed species, 5000 non-uniformly distributed interpolated data points were considered, spanning a range from 0 to 6000 s (equivalent to 1 h and 40 min).

Table 1 summarizes the experimental conditions attributed to PROCODA.

Table 1. Experimental parameters used as input to PROCODA Code.

Flux of radiation	1×10^9 projectiles cm^{-2} s^{-1}
Projectile energy	4×10^7 eV
N_2 initial column density	9.8×10^{17} molecules cm^{-2}
Ice thickness	0.62×10^{-4} cm
Ice density	0.84 g cm^2
Sample area	0.55 cm^2
Total desorption yield	1×10^4
Sample temperature	15 K

2.2 The PROCODA code

The PROCODA code, as detailed by Pilling et al. (2022), was developed to solve a system of interconnected differential equations, depicting the chemical evolution of typical astrophysical ices under ionizing radiation exposure. The code yields numerical values for ERCs, synonymous with rate constants (k) for gas-phase reactions, along with molecular abundances of observed and predicted species, and vital information for radiation-induced desorption into the gas phase. Although the proposed reactions illustrate the expected physical and chemical processes within the ice, they may not strictly adhere to elementary reactions. Because of this, their rate constants (or coefficients) are termed effective (apparent), with each effective reaction rate accounting for the availability of involved reactants (N_i) up to the second order. Further details regarding the current version of the code are available in Pilling et al. (2023a).

In the system of coupled chemical reactions and desorptions addressed by the code, the variation of the column density (dN_i/dt) for each molecule i present in the system is calculated from the following equation:

$$\frac{dN_i}{dt} = -\mathrm{DES}_i(t) - \sum_{d1} k_{d1} N_i(t) - \sum_{d2} k_{d2} N_i(t) N_a(t)/L + \sum_{p1} k_{p1} N_a(t) + \sum_{p2} k_{p2} N_a(t) N_b(t)/L \ \ [\text{molecules cm}^{-2}\ \text{s}^{-1}] \quad (1)$$

where, k is the effective rate constant, letters 'd' and 'p' refer to destruction and productions processes, respectively, numbers 1 and 2 refer to unimolecular or bimolecular processes, respectively, N is the column density and N is the ice thickness.

Equation (1) provides a comprehensive description of the variation in column density of a given species over time. Formulated in terms of a rate law, this equation encompasses the desorption rate of molecule i from the ice surface, as well as the production and consumption rates of molecule i. The first term in equation (1), $\mathrm{DES}_i(t)$, represents the desorption of molecule i from the ice to the gas phase, a consequence of incoming radiation. The $\mathrm{DES}_i(t)$ calculation is contingent upon the column density of species i, in addition to the intrinsic desorption rate ($k_{des,i}[s^{-1}]$) and the dimensionless surface coverage of the species i as a function of time ($\Omega_i(t)$), and it's given by: $\mathrm{DES}_i(t) = k_{des,i}\ \Omega_i(t)\ N_i(t)$. The second and third terms are associated with the destruction (or consumption) of molecule i, with the distinction lying in the underlying cause. The second term is associated with the destruction (or consumption) of molecule i, induced by radiation, an unimolecular process. In contrast, the third term is associated with the destruction (or consumption) of molecule i due to collisions between molecule i with any other molecule (e.g. molecule 'a'), a bimolecular process. The fourth and fifth terms are similar to the second and third terms; however, these terms are associated with the production ('p') of molecule i. While in fourth term, molecule i is produced by the irradiation of another molecule (e.g. molecule 'a'), an unimolecular process, in the fifth term, molecule i is produced from the collision of other two species (e.g. molecules 'a' and 'b'), a bimolecular process.

In essence, the PROCODA code minimizes a function known as the score function (SF), which accesses the system's closeness to its optimal global solution, considering the adaptable weights assigned

to different constraints.

$$\mathrm{SF} = \sum_i p_i \times \frac{(oN_{i,\mathrm{data}} - oN_{i,\mathrm{model}})^2}{oN_{i,\mathrm{data}}} + p_j \times \left[(1 - \mathrm{MSC}_f) + (1 - \mathrm{MSCo}_f) + (1 - \mathrm{MSCo}_m)\right] + p_k \times (1 - \mathrm{DSC}) + p_z \times (1 - \mathrm{SSC}). \quad (2)$$

The score function (SF) shown in equation (2) determines different sources of discrepancies between the computed values and the available experimental data. The parameters p_i, p_j, p_k, and p_z are the weight (dimensionless) of each term described in equation (2). These parameters allow for the search of the best solution during the computational minimization processes and are selected arbitrarily and manually until until the *SF* reaches its lowest possible value during the minimization process, as well as a very small value for the χ^2 function (a function obtained directly from equation (2) by setting $p_i = 1$ and $p_j = p_k = p_z = 0$) for observed molecular species at the end of the calculation. The first term in equation (2) is a root mean square error (RMSE) for each observed species ($i = \{H_2O, N_2, NO, N_2O, NO_2\}$), calculated in order to evaluate the discrepancy between the experimental values of column density ($oN_{i,\mathrm{data}}$) and the column density values calculated by the model ($oN_{i,\mathrm{model}}$). The parameters p_i of particular significance for species that are less abundant. All other terms in equation (2) are related to the similarity criterion (SC), which can be calculated using equation (3):

$$\mathrm{SC} = 1 - \frac{|n1 - n2|}{|n1 + n2|}. \quad (3)$$

The term MSC_f in the SF denotes the column mass SC, calculated considering the similarity between the initial column mass of the modelled system and the total column at the end. The values of $\mathrm{MSC}o_f$ and $\mathrm{MSC}o_m$ represent the column mass similarity criterion between the experimentally observed column mass and the observed column mass in the model at the final (f) of modelling time and at the middle (m) of the modelling time. These terms are important to guarantee the mass conservation by applying large values of p_j. The parameter DSC stands for the 'desorption similarity criterion', calculated considering the similarity between the experimental desorption yield and the total molecular desorption yield computed by the model, where large p_k ensures that the model desorption yield is closely approximated by the estimated value. Finally, the parameter SSC is the slope similarity criterion, which is related to the achievement of the chemical equilibrium phase in the ice, as explained by Pilling et al. (2022), the large similarity in this criterion implies that the column masses of both observed and non-observed species reach a sloped plateau at a high level of irradiation over time, reaching the CE stage, where large p_z guarantees the CE stage at final fluences. For a more thorough exposition of the calculation of SSC, refer to the work of Pilling et al. (2022).

To model the H_2O:N_2 ice, we considered a total of 930 coupled chemical reactions, including the reactions of desorption, occurring in the ice and producing 28 species. All the details about the equations set are given in the supplementary material.

Table 2 presents all the chemical species used in this study and their corresponding gas-phase formation enthalpies at 0 K taken from Branko Ruscic (2024). In the first phase, the thermochemistry data was used for the chemical species to obtain the best-fitting model and provide the first values for the ERCs. Starting from the best solution from the first phase, in the second phase the thermochemistry data was turned off and a new calculation took place using the ERCs obtained in the first phase as an initial guess.

Table 2. Chemical species and gas-phase formation enthalpies at 0 K ($\Delta_f H^0$) considered in this work.

Species	$\Delta_f H^0$ (kcal mol^{-1})	Species	$\Delta_f H^0$ (kcal mol^{-1})
H	216.034	HO_2	15.09
H_2	0.00	H_2O_2	−129.417
N	470.577	N_3	452.24
O	246.844	N_2O	86.022
OH	37.279	NO_2	36.878
NH_3	−38.563	HNO_2	−72.971
H_2O	−238.902	O_3	144.407
NH_4	643.03	HO_3	90.76
H_3O	605.88	N_2O_2	172.93
N_2	0.00	NO_3	79.4
N_2H_2	207.12	HNO_3	−124.48
NO	90.639	N_2O_3	90.76
HNO	109.95	N_2O_4	20.19
O_2	0.00	N_2O_5	24.35

The current version of the code is structured into two phases: Phase 1 conducts calculations based on the ERCs ordering hypothesis, while Phase 2 disregards this hypothesis but refines the best solution from Phase 1. The ordering hypothesis comprises two conditions: ordering within reaction groups (OG), assuming that more exothermic reactions have higher rate constants, and ordering within single reactions (OS), where the most exothermic reactions are expected to proceed faster. The details about the ERCs calculation can be read at Pilling et al. (2023a).

2.3 Advantages and limitations of the code

The PROCODA code has the advantage of mapping the experimentally observed species in infrared spectra and the non-observed species, which includes molecules that have not been characterized in practical experiments, and molecules that have not yet been observed in the ISM, or even species that are difficult to be measured, such as atomic and diatomic species. PROCODA models the reactions induced by irradiation and bimolecular collision reactions. Finally, PROCODA provides the abundances of both observed and unobserved species as a function of time and the desorption rate of each species.

Despite the advantages of the code, it also has limitations. The current version of the code assumes that all reactions are elementary, i.e. the overall order of the reaction is given by the sum of the amounts of reactants in each reaction. Also, the current version of the code does not consider ionic or excited species. These are implicitly included in the reactions present in the mechanism, which are therefore considered to be effective reactions in terms of the physiochemical processes, and not necessarily elementary processes.

However, even with the presented limitations, the code may still provide meaningful insights regarding the kinetics, relative abundances, and desorption of chemical species in N_2-rich astrophysical ices subjected to cosmic rays.

3 RESULTS

This section presents and analyses the main findings, with a particular emphasis on the chemical equilibrium. The potential alterations to the mechanisms, the possible intermediates, and the desorption processes will be addressed in greater depth in a forthcoming publication, which will provide a more comprehensive and detailed understanding of the subject matter.

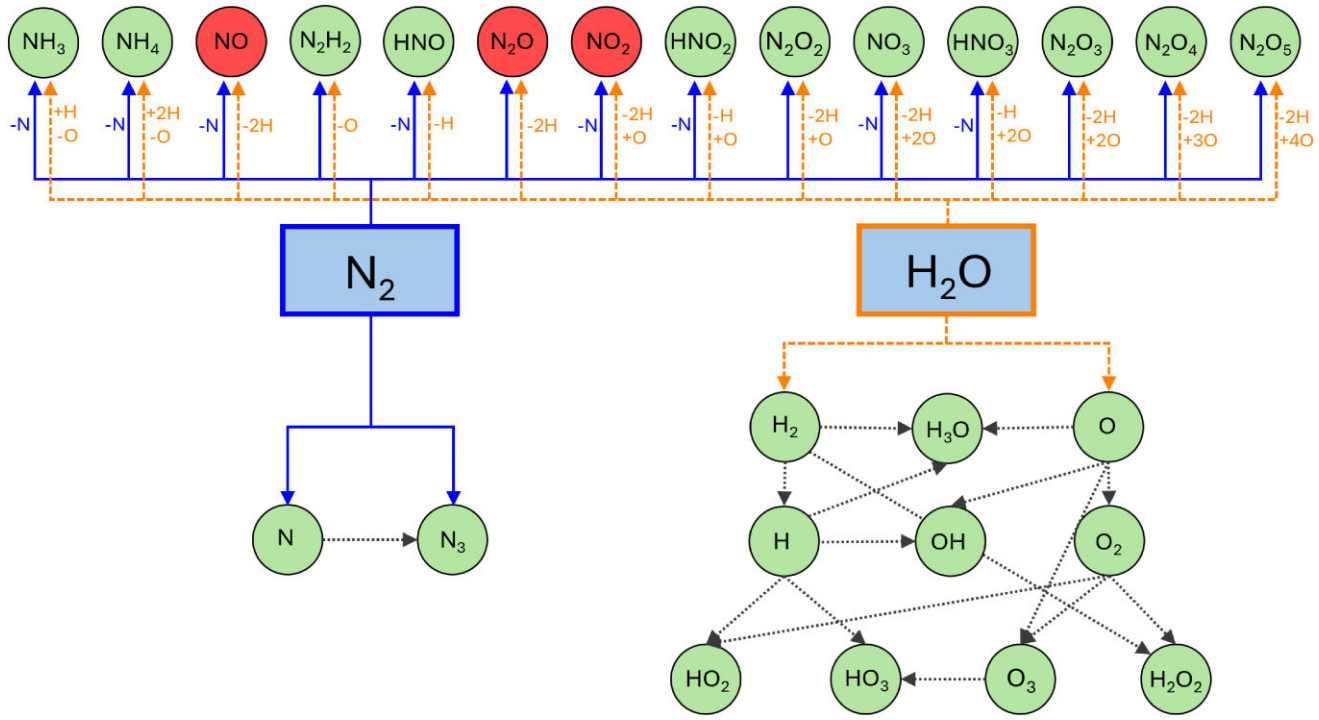

Figure 1. Scheme of the reaction network employed in this work (simplified version). The rectangles represent the parent species (original ice composition). The circles represent the daughter species (the other 26 modelled species apart from the parent species). The circles filled with red are the experimentally observed species, while the circles filled with green are the experimentally non-observed species. The solid blue line represents the contribution of N_2 to the formation of the daughter species. The dashed orange line represents the contribution of H_2O to the formation of the daughter species. The dark grey dotted line represents the contribution of one species to the formation of another one. This figure is just an example of how the chemical reactions are coupled but all of the 28 species can react between themselves.

As previously mentioned, it was modelled a total of 930 coupled chemical reactions occurring in the ice resulting in the production of 28 possible species (H, H_2, N, O, OH, NH_3, H_2O, NH_4, H_3O, N_2, N_2H_2, NO, HNO, O_2, HO_2, H_2O_2, N_3, N_2O, NO_2, HNO_2, O_3, HO_3, N_2O_2, NO_3, HNO_3, N_2O_3, N_2O_4, and N_2O_5). Fig. 1 represents a simplified scheme of the reaction network employed in this work.

3.1 Best-fitting model

The modelled abundances for all species are presented in Fig. 2. The figure demonstrates a correlation between the experimental data and the optimal fit for the specified observable species. The dashed line represents the modelled summed column density for desorbed species. The quality of the fit was evaluated using the calculated summed chi-square function (χ^2), which compares the observed species column densities in the experimental data set with the calculated column densities in the model. The best-fitting model yielded a summed desorption yield of 1.17×10^5 molecules ion^{-1} and a value of 6.282 for the summed χ^2 function. Table S1 in the supplementary information material, provides all the forward, reverse, and desorption values obtained from the best-fitting model. There, one can find information about the calculated ERCs or 'k' values and branching ratios (BR (per cent)), as well as the enthalpy of the reaction in gas phase ($\Delta_r H$, 0 K).

An alternative version for Fig. 2 is available in the Supporting Information (Fig. S1), in which the same data is presented in a log–log plot, thereby enabling reader to analyse the initial evolution of the system, as well as the intermediates present in the reaction chain. As one can see from Fig. S1, the code does not adequately describe the initial seconds of the reaction; however, it describes the reaction adequately after the first 100 s. As previously mentioned, part II of this series of work will delve deeper into the reaction mechanism.

3.2 Abundance at chemical equilibrium

A quasi-equilibrium phase, characterized by evolutionary time-scales that are substantially longer than those observed at the initial stage, was obtained after ≈5000 s with constant ion bombardment and temperature (15 K). This corresponds roughly to the ion fluence of 2×10^5 Ni^{11+} ions cm^{-2} ($= 8 \times 10^{12}$ eV cm^{-2}). The quasi-equilibrium phase can be verified in Fig. 2, where it is evident that some species continue to evolve even after a protracted period of chemical reaction. Despite the presence of a 'quasi-equilibrium' phase, the term 'chemical equilibrium' will be employed for simplicity's sake.

Fig. 3 depicts the percentage of the molecular abundance of each species present on the ice surface at chemical equilibrium. The species were classified into four categories: the parent species (N_2 and H_2O) are represented in blue, while the species initially considered 'experimentally observed' based on the work of Barros et al. (2015; NO, N_2O, and NO_2) are shown in red. The species modelled computationally but not experimentally observed are represented by, while the species with low abundance (lower than 1×10^{-4} per cent) are shown in black. In this study, given that species with a column density below 0.01 per cent are not important to the chemical equilibrium, the data analysis will be concentrated on species with a column density higher than 0.01 per cent, as illustrated by the black and dashed lines.

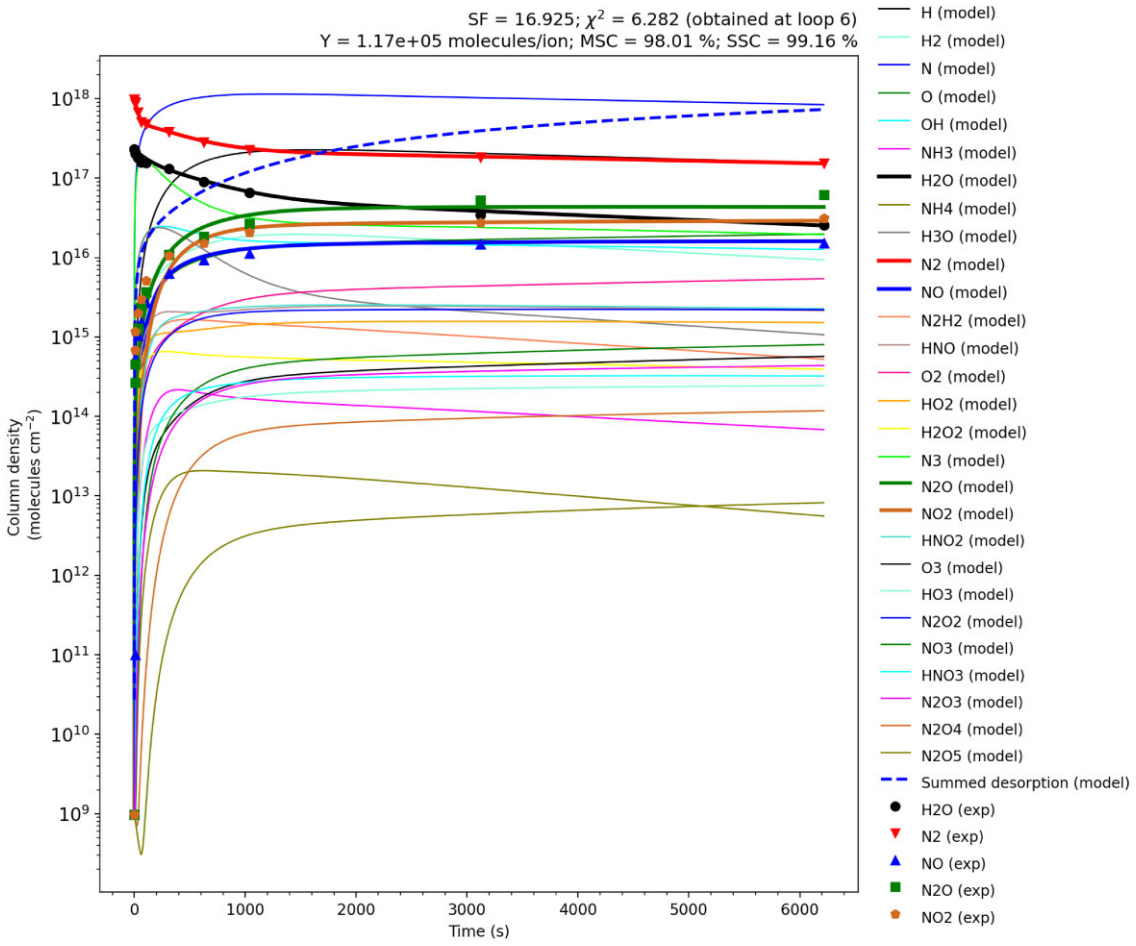

Figure 2. Column density over time obtained for the best-fitting model employing the PROCODA code on 15 K H_2O:N_2 (1:5) ice irradiated by cosmic rays (40 MeV Ni^{11+}). Thick lines show the model for the observed species. Thin lines show the model for non-observed species. Experimental data are represented by the symbols. Some model parameters are presented in the header. The dashed blue line represents the summed desorption as a function of time.

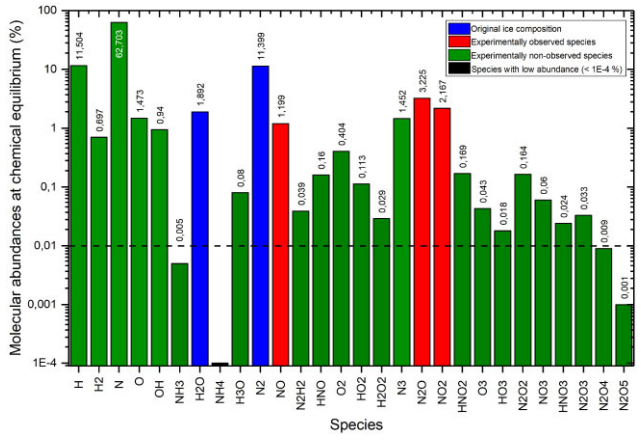

Figure 3. Molecular abundance (per cent) of each of the 28 modelled species at equilibrium. In blue, are the reactants (father species). In red are the experimentally observed species (daughter species). In green are the experimentally non-observed species. In black the species with low abundance ($< 1 \times 10^{-4}$).

First, analysing the parent species, it is possible to observe that at the end of the experiment, the H_2O:N_2 ratio remained close to the initial proportion (5:1). Examining the experimentally observed species (NO, N_2O, and NO_2), it is possible to see that all of them exhibit a significant amount at equilibrium, with N_2O being the most abundant among the three, followed by NO_2 and NO, respectively.

Concerning the non-observed species, the methodology employed is of great consequence in the acquisition of data about species that are undetectable by FTIR, such as atoms (H, O, and N) and diatomic molecules devoid of a dipole moment variation (H_2 and O_2). It can be observed that these species are present in significant concentrations on the surface, with atomic nitrogen being the most abundant species (62.70 per cent), followed by atomic hydrogen (11.50 per cent), atomic oxygen (1.47 per cent), molecular hydrogen (0.70 per cent), and molecular oxygen (0.40 per cent).

Other non-experimentally observed species that showed significant abundance were, from most to least abundant: N_3, OH, HNO, N_2O_2, HNO_2, and HO_2, in this order. It is worth noting that, consistent with literature experiments, N_3 is indeed an abundant species; however, it was not the most abundant species found among the 28 modelled species.

Barros et al. (2015), in her work, characterized HNO, HNO_2, and HNO_3 but did not quantify them. In this work, it is possible to observe that all of these three species presented abundances above 0.1 per cent

Table 3. Molecular abundance at chemical equilibrium. Calculated (Calc.) using PROCODA versus experimental (Exp.) values.

Species	Calc. N_f	Exp. N_f
H	1.5	–
H_2	9.3×10^{-2}	–
N	8.4	–
O	2.0×10^{-1}	–
OH	1.3×10^{-1}	–
NH_3	6.8×10^{-4}	–
H_2O	2.5×10^{-1}	0.05
NH_4	5.6×10^{-5}	–
H_3O	1.1×10^{-2}	–
N_2	1.5	1.3
NO	1.6×10^{-1}	0.158
N_2H_2	5.2×10^{-3}	–
HNO	2.1×10^{-2}	–
O_2	5.4×10^{-2}	–
HO_2	1.5×10^{-2}	–
H_2O_2	3.9×10^{-3}	–
N_3	2.0×10^{-1}	0.530
N_2O	4.3×10^{-1}	0.653
NO_2	2.9×10^{-1}	0.357
HNO_2	2.3×10^{-2}	–
O_3	5.7×10^{-3}	0.026
HO_3	2.4×10^{-3}	–
N_2O_2	2.2×10^{-2}	–
NO_3	8.0×10^{-3}	0.177
HNO_3	3.2×10^{-3}	0.002
N_2O_3	4.4×10^{-3}	0.003
N_2O_4	1.2×10^{-3}	0.009
N_2O_5	8.2×10^{-5}	0.017

Notes. The initial column density (N_0) for H_2O nad N_2 considered in this work was identical to that used by Barros et al. (2015): 2.3×10^{17} molecules cm^{-2} and 9.8×10^{17} molecules cm^{-2}, for H_2O and N_2, respectively.
N_f represents the final column density and is given in 10^{17} molecules cm^{-2}. Experimental data were taken from Barros et al. (2015).

(0.160 per cent, 0.169 per cent, and 0.02 per cent, respectively). It is also possible to see that the formation of N_2O_4 and N_2O_5 is not favoured.

Fig. 3 also illustrates that species crucial for life, such as NH_3 and NH_4 did not exhibit significant abundance at chemical equilibrium, with NH_3 presenting a column density lower than 0.01 per cent and NH_4 a column density lower than 1×10^{-4}.

Table 3 shows the calculated column density of the species present in the system at chemical equilibrium, as well as the column density obtained through experimental analysis, as referenced by Barros et al. (2015).

It is interesting to note that in the current work, at the end of the experiment, the H_2O:N_2 ratio remained close to the initial ratio of 1:5, whereas the experimental result shows a substantial change (1:26), with the water abundance being much lower than some of the daughter species, such as N_2O, N_3, NO_2, NO_3, and NO.

3.3 Molecular desorption

Fig. 4, in turn, shows the percentage of each desorbed species in the last second of the reaction. The colours follow the criteria previously defined in Fig. 3, with blue representing the parent species (N_2 and H_2O), red representing the species initially considered 'experimentally observed' based on the work of Barros et al. (2015; NO, N_2O, and NO_2) and green representing the 'experimentally non-observed' species. In this column graph, some species are also shown

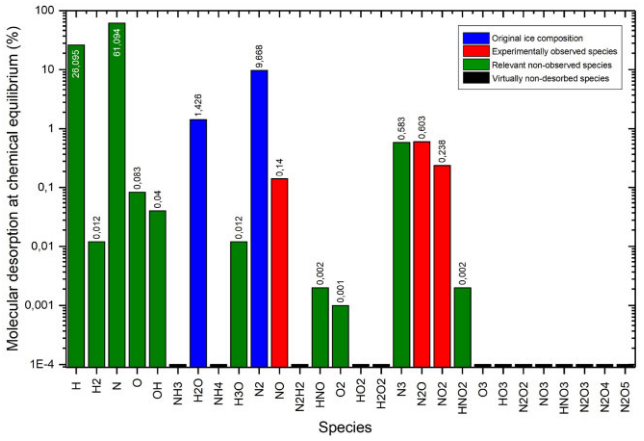

Figure 4. Molecular desorption (per cent) of each of the 28 modelled species at the end of the experiment. The colours follow the rules used in Fig. 3. In blue are the reactants (father species). In red are the experimentally observed species (daughter species). In green are the experimentally non-observed species. In black are the experimentally non-observed species that did not show significant desorption ($< 1 \times 10^{-4}$ per cent).

in black, representing those with a molecular desorption rate lower than 10^{-4} per cent.

Regarding the parent species (N_2 and H_2O) and the experimentally observed species (NO, N_2O, and NO_2), all of them exhibited desorption from the ice. Among the species non-experimentally observed NH_3, NH_4, N_2H_2, HO_2, H_2O_2, O_3, HO_3, N_2O_2, NO_3, HNO_3, N_2O_3, N_2O_4, and N_2O_5 did not exhibit significant surface desorption (virtually non-desorbed species).

Higher-order oxides such as N_2O_4 and N_2O_5, in addition to having low surface abundance (as shown in Fig. 3), also did not show significant desorption, indicating that the small amount produced is not desorbed, remaining trapped in the ice. This could suggest that these species are formed in the ice bulk.

It is also important to emphasize that the ice surrounding will be full of atomic H and N. Consequently, there will be several reactions occurring in the gas phase that will contribute to the formation of more N-bearing species. The aspects of the gas-phase reactions will be more detailed in the following parts of this series of studies. This paper discusses the desorption patterns with respect to fluency and proposes potential gas-phase chemical reactions that could occur near grain surfaces. By understanding these reactions, we can better comprehend the chemical reaction network that contributes to the understanding of complex regions such as star and planet forming regions.

3.4 First insight into the mechanism involving the parent species

In this section, we do a brief overview on the mechanism involving the main species observed in this work. We considered 'main' species those with high abundance, those acting as important reaction intermediates, and those with relevant significance in astrophysical implications. In this sense, this section will discuss the dominant pathways related to the formation and/or consumption of the parent species (N_2 and H_2O) at the start and end of the experiment, while the main daughter species (NO, N_2O, NO_2, N_2O, NH_3, HNO, HNO_2, and H_2O_2) will be analysed only at the end of the experiment. A deeper analysis will be carried out in a forthcoming paper (Part II).

Initially ($t = 0s$), there are only the parent species. In this sense, there are three options to start the reactions: (1) N_2 is irradiated, (2) H_2O is irradiated, or (3) there's a biomolecular collision between N_2 and H_2O. In the first case, if N_2 is bombarded with CR, then there's only one possible reaction to occur: the formation of atomic nitrogen, as shown in equation (4)

$$N_2 + R \xrightarrow{k_9} N + N$$
$$k_9 = 2.0 \times 10^{-4}\ s^{-1}. \quad (4)$$

In the second case, however, if H_2O is bombarded by CR, then two options exist: (I) the formation of atomic hydrogen and hydroxil radical, or (II) the formation of diatomic hydrogen and atomic oxygen, as shown on equations (5) and (6), respectively.

$$H_2O + R \xrightarrow{k_{17}} H + OH$$
$$k_{17} = 6.1 \times 10^{-5}\ s^{-1}$$
$$(\text{BR per cent} = 75.53 \text{ per cent}) \quad (5)$$

$$H_2O + R \xrightarrow{k_{33}} H_2 + O$$
$$k_{33} = 2.0 \times 10^{-5}\ s^{-1}$$
$$(\text{BR per cent} = 24.47 \text{ per cent}). \quad (6)$$

Equation (5) can be classified as more important than equation (6), once equation (5) presents a higher branching ratios (BR = 75.53 per cent), and it makes sense, since the molecule of H_2O in equation (5) is supposed to break only an OH bond, while the molecule of H_2O in equation (6) needs first to break two OH bond and only then the H will bind to the other H and break the second OH bond. In other words, equation (6) is probably not an elementary reaction. Another possibility to produce H_2 and O, equation (5) can be followed by equation (7), which, as one can see, is not a favorable pathway due to its low branching ratio (BR per cent = 7.14 per cent). Instead, H and OH react to restore the water molecule (BR per cent = 92.86 per cent).

$$H + OH \xrightarrow{k_{61}} H_2 + O$$
$$k_{61} = 3.8 \times 10^{-26}\ cm^3\ molecules^{-1}\ s^{-1}$$
$$(\text{BR per cent} = 7.14 \text{ per cent}) \quad (7)$$

$$H + OH \xrightarrow{k_{18}} H_2O$$
$$k_{18} = 5.0 \times 10^{-25}\ cm^3\ molecules^{-1}\ s^{-1}$$
$$(\text{BR per cent} = 92.86 \text{ per cent}). \quad (8)$$

Finally, the third option regarding the parents species would be the collision between H_2O and N_2 (equation 9).

$$H_2O + N_2 \xrightarrow{k_{184}} H_2 + N_2O$$
$$k_{184} = 3.6 \times 10^{-27}\ cm^3\ molecules^{-1}\ s^{-1}. \quad (9)$$

Considering the fact that, in the condensed matter, the molecules are not floating at high speed, they are practically frozen, and the collision between molecules is hindered. Even taking into consideration the 'liquid ice region' formed around the CR pathway (Vasconcelos et al. 2017b), the effective collision of these two inert molecules is not favoured. Also, equation (9) is not an elementary process, it should occur in steps. These factors explain the low value obtained for this ERC (k_{184}).

In this sense, reactions represented by equations (4) and (5) may dominate the mechanism in the first seconds of the experiment, when no other daughter species have been abundantly produced.

Table 4. Average values for reaction rates and desorption.

Average parameter	N_2:H_2O ice at 15 K irradiated by 40 MeV Ni^{11+} (This work)	Pure H_2O ice at 13 K irradiated by 52 MeV Ni^{11+} (Pilling et al. 2023b)
ERC for radiation-induced dissociation	$3.7 \times 10^{-3}\ s^{-1}$	$2.5 \times 10^{-2}\ s^{-1}$
ERC for bimolecular collisions	$2.7 \times 10^{-25}\ s^{-1}\ cm^3 molecules^{-1}$	$4.3 \times 10^{-24}\ s^{-1}\ cm^3\ molecules^{-1}$
ERC for intrinsic desorption	$5.4 \times 10^{-4}\ s^{-1}$	$3.2 \times 10^{-6}\ s^{-1}$
Desorption rate	$6.4\ 10^{13}$ molecules s^{-1}	1.7×10^{13} molecules s^{-1}
Desorption yield	$1.2\ 10^5$ molecules ion^{-1}	1.0×10^4 molecules ion^{-1}

3.5 Comparison with previous work

Table 4 presents the average values for the ERCs, desorption rate, and desorption yield derived from the best-fitting model used in this study, alongside those reported by Pilling et al. (2023b), which applied a similar methodology. These values serve as a benchmark for validating the code. Despite differences in ice composition between the two studies, the temperature and radiation conditions were comparable, and the ERC values obtained in both works remained closely aligned.

The ERCs, with the exception of the one for the intrinsic desorption reactions, were lower than those previously calculated for pure H_2O ice. This difference may be attributed to the presence of more complex molecules, which could exhibit reduced diffusion within the ice bulk under irradiation. The average desorption rate and yield in this work were higher than those calculated for pure H_2O ice, a behaviour that Part III (in prep) of this study series may help to elucidate further.

4 ASTROPHYSICAL IMPLICATIONS

The PROCODA code represents a valuable tool for the astrochemical community, as it allows the kinetic description of reactions occurring in astrophysical ices under irradiation. It can describe not only reactions involving species already observed experimentally but also those not yet detected. This offers valuable insights into the composition of ice in the interstellar medium thousands of years ago and possible future scenarios.

One particularly important application of the PROCODA code is in studying the behaviour of key molecules such as molecular nitrogen in the ISM. The presence of these species in the ISM plays a crucial role in not only supporting life. Once the identification of N-bearing species is complete, insights may be gained on the formation of important structures, such as simple amino acids (Vasconcelos et al. 2017a). Furthermore, these species drive activity on icy surfaces. For instance, N_2 plays a analogous to that of water on Earth, functioning as the primary volatile on Pluto that drives activity on the icy surface (Glein & Waite 2018). In this regard, the ice under investigation is pertinent to astrophysical ices observed in regions of the ISM that are less exposed to radiation, such as trans-Neptunian objects. Despite the difficulty in detecting gaseous N_2 in space, the solid-state form of N_2 has been identified as the primary surface component of Pluto and Triton (Neptune's largest moon). For further details, please refer to

the following sources: Cruikshank et al. (1993), Owen et al. (1993), and Bernstein & Sandford (1999).

Therefore, this study simulates the chemical reactions occurring in H_2O:N_2 ice when exposed to radiation, resulting in the formation of various species, including both those previously detected in the ISM and those not yet observed. The data provided by this work suggest that the daughter species, particularly the N-bearing ones considered 'non-observed,' could be promising candidates for future ISM detections using the JWST and the Atacama Large Millimeter/submillimeter Array (ALMA), as their presence indicates N_2 in cosmic objects impacted by cosmic ray bombardment.

In this manuscript, we modelled a total of 28 species as a consequence of the radiolysis of H_2O:N_2 (1:5) at 15 K, to gain insight into the chemical processes that occur in the interstellar medium. However, of all the N-bearing species modelled in this work, only five of them have been detected in the interstellar medium to date. NH_3 was first identified in the supermassive black hole at the Galactic Center of the Milky Way, Sagittarius A (Sgr A), in 1968 by Cheung et al. (1968), and also the only one to be identified in interstellar ices, first by Lacy et al. (1998) in 1998, by Gibb et al. (2004) in 2004, and Bottinelli et al. (2010) in 2010.

In 1997, Ulich, Hollis & Snyder (1977) observed HNO in the giant molecular cloud, Sagittarius B2 (Sgr B2), localized in the Milky Way, close to the Galactic Center, and also in an emission nebula localized in the constellation of Orion. Later, in 1993, Snyder et al. (1993), observed HNO again in other four interstellar clouds: L134N, W33A, W51M, and DR21. The detection of HNO was confirmed by Ziurys, Hollis & Snyder (1994a) with the addition of a new source: the Flame Nebula (NGC 2024).

Among the gas phase inventory towards Sgr B2, it was also detected the molecule NO (Liszt & Turner 1978) and the molecule N_2O (Ziurys et al. 1994b; Halfen, Apponi & Ziurys 2001). Besides, considering the five N-bearing molecules already detected in the interstellar medium, in the present work, N_2O was the most abundant one, being a good candidate for future attempts at solid-phase astronomical observations, together with NO. As suggested by Ioppolo et al. (2020), pure NO and NO_2 ice are not expected to exist in space, however interstellar NO and NO_2 should be present in the solid phase mixed with more abundant species.

Recently, gaseous HNO_2 was identified in the component B of the low-mass protostellar binary IRAS 16293-2422, located at a distance of $\approx$ 140 pc in the ρ Ophiuchus cloud complex (Dzib et al. 2018), by Coutens et al. (2019).

It is also noteworthy, that in this study, NO_2 was modeled as the second most abundant molecule, despite not yet being detected in the ISM. This finding also positions NO_2 as a promising candidate for future astronomical observations. The studied N-compounds such as N_2O and NO can act as tracer molecules to derive the abundances of the nitrogen molecule in interstellar and solar system ices as also highlighted by Jamieson et al. (2005).

Moreover, the PROCODA code effectively models the kinetics that regulate chemical equilibrium within reaction networks, thereby providing valuable insights into past and future compositions of specific ISM regions. A deeper analysis of the preferential chemical routes for both formation and consumption of the studied species in the bombarded H_2O:N_2 ice will be carried out in a forthcoming paper (Part II).

The ERCs calculated in this work could significantly benefit programs, such as PRODIMO and NAUTILUS, that utilize rate coefficients to simulate the chemical evolution of astrophysical environments in the interstellar medium. The rate coefficients produced by PROCODA are particularly valuable because they include kinetic constants for non-observable species, extending beyond experimental parameters and enhancing the accuracy and detail of kinetic models. This contribution supports a more comprehensive mapping of ice evolution in cold ISM regions and on satellite surfaces covered by ice.

Considering that the surroundings of the ice will be full of atomic species, a whole chain of reactions will occur in the gas phase that will contribute to the formation of more species of N despite those modeled in this work. In addition, some N-bearing species will also be in the ice surroundings, including those not yet detected in the ISM, such as NO_2 and N_3, making them, once again, potential molecules for astronomical observations. In this sense, the desorption rates are also essential for understanding how molecules are transferred from interstellar ices to the gas phase and how they contribute to the understanding of complex regions such as star and planet-forming regions. The part II of this series of studies will go deeper into the radiation-induced desorption processes and the molecular species named as good candidates to be observed with radio-telescopes.

5 CONCLUSIONS

In this work, 28 molecules and 930 reactions were employed to describe the chemical evolution of a N_2–H_2O ice irradiated by cosmic ray analogues (40 MeV) using the PROCODA code. The main conclusions were as follows:

(i) We were able to quantify the abundances over time of experimentally observed and experimentally non-observed (predicted) species produced in the ice due to the ion bombardment. The five species most produced in the chemical equilibrium phase were: N (62.7 per cent), H (11.5 per cent), N_2O (3.2 per cent), NO_2 (2.2 per cent), and O (1.5 per cent) becoming good candidates for detection in astronomical environments.

(ii) The largest molecule produced was N_2O_5, with an abundance of only 0.001 per cent. In addition, N_2O_5 has shown low desorption from the ice surface, suggesting that large molecules, in addition to being difficult to produce, could be produced in most of the ice and kept inside rather than being desorbed.

(iii) The formation of NH_3 from the radiolysis of the studied ice was very low. This suggests that reaction routes to sustain the observed NH_3 abundances in ISM and other astrophysical ices should be different than the one studied in this work.

(iv) The main desorbed species were N (61.1 per cent), H (26.1 per cent), N_2 (9.7 per cent), H_2O (1.4 per cent), and N_2O (0.6 per cent). In an astrochemical scenario, these species will probably participate in gas-phase reactions in the ice surroundings, contributing to the increase of the chemical complexity.

Finally, this work provided parameters (e.g. coefficient rates) to be used in models of chemical evolution in astrophysical environments in the presence of ionizing radiation, such as ices towards Sagittarius B2 (and other molecular clouds), protostellar ices, and solar system ices. In addition, all the experimentally non-observed or non-detected species discussed in this work may be targets of future astronomical observations with modern telescopes, such as the JWST and the ALMA telescopes.

ACKNOWLEDGEMENTS

This study was financed by the Coordenação de Aperfeiçoamento de Pessoal de Nível Superior – Brasil (CAPES) – Finance Code 001. The Conselho Nacional de Desenvolvimento Científico e

Tecnológico (CNPq) – projects nos. 302608/2022-2, 350323/2024-0, 163539/2024-3, 350054/2023-1, 407124/2022-5, and 316874/2023-0, and by Fundação de Amparo à Pesquisa do Estado de São Paulo (FAPESP) under grant no. 2024/05115-5.

CONFLICTS OF INTEREST

The authors declare that they have no known competing financial interests or personal relationships that could have appeared to influence the work reported in this paper.

DATA AVAILABILITY

The data underlying this article will be shared on reasonable request to the corresponding author.

REFERENCES

Bernstein M. P., Sandford S. A., 1999, Spectrochim. Acta Part A: Mol. Biomol. Spectrosc., 55, 2455
Bottinelli S. et al., 2010, ApJ, 718, 1100
Branko Ruscic D. H. B., 2024, ATcT Thermochemical Values ver. 1.128—atct.anl.gov. Available at: https://atct.anl.gov/Thermochemical%20Data/version%201.128/index.php
Cheung A. C., Rank D. M., Townes C. H., Thornton D. D., Welch W. J., 1968, Phys. Rev. Lett., 21, 1701
Coutens A. et al., 2019, A&A, 623, L13
Cruikshank D. P., Roush T. L., Owen T. C., Geballe T. R., de Bergh C., Schmitt B., Brown R. H., Bartholomew M. J., 1993, Science, 261, 742
de Barros A. L. F., Silveira E. F. d., Bergantini A., Rothard H., Boduch P., 2015, ApJ, 810, 156
Dzib S. A. et al., 2018, A&A, 614, A20
Gibb E. L., Whittet D. C. B., Boogert A. C. A., Tielens A. G. G. M., 2004, ApJS, 151, 35
Glein C. R., Waite J. H., 2018, Icarus, 313, 79
Halfen D. T., Apponi A. J., Ziurys L. M., 2001, ApJ, 561, 244
Hudson R. L., 2018, ApJ, 867, 160
Ioppolo S., Kaňuchová Z., James R. L., Dawes A., Jones N. C., Hoffmann S. V., Mason N. J., Strazzulla G., 2020, A&A, 641, A154
Jamieson C. S., Bennett C. J., Mebel A. M., Kaiser R. I., 2005, ApJ, 624, 436
Lacy J. H., Faraji H., Sandford S. A., Allamandola L. J., 1998, ApJ, 501, L105
Liszt H. S., Turner B. E., 1978, ApJ, 224, L73
Owen T. C. et al., 1993, Science, 261, 745
Pilling S., Carvalho G. A., Rocha W. R. M., 2022, ApJ, 925, 147
Pilling S., Rocha W. R. M., Carvalho G. A., de Abreu H. A., 2023a, Adv. Space Res., 71, 5466
Pilling S., Carvalho G. A., de Abreu H. A., Galvão B. R. L., da Silveira C. H., Mateus M. S., 2023b, ApJ, 952, 17
Quirico E., Douté S., Schmitt B., de Bergh C., Cruikshank D. P., Owen T. C., Geballe T. R., Roush T. L., 1999, Icarus, 139, 159
Snyder L. E., Kuan Y.-J., Ziurys L. M., Hollis J. M., 1993, ApJ, 403, L17
Ulich B. L., Hollis J. M., Snyder L. E., 1977, ApJ, 217, L105
Vasconcelos F. A., Pilling S., Rocha W. R. M., Rothard H., Boduch P., 2017a, Phys. Chem. Chem. Phys., 19, 24154
Vasconcelos F. d. A., Pilling S., Rocha W. R. M., Rothard H., Boduch P., 2017b, ApJ, 850, 174
Ziurys L. M., Hollis J. M., Snyder L. E., 1994a, ApJ, 430, 706
Ziurys L. M., Apponi A. J., Hollis J. M., Snyder L. E., 1994b, ApJ, 436, L181

SUPPORTING INFORMATION

Supplementary data are available at *MNRAS* online.

Supporting_Information_-_Characterization_of_H2ON2_ice_under_bombardment_by_cosmic_rays_Part_1_Final Version.pdf.

Please note: Oxford University Press is not responsible for the content or functionality of any supporting materials supplied by the authors. Any queries (other than missing material) should be directed to the corresponding author for the article.

This paper has been typeset from a TEX/LATEX file prepared by the author.